PHYSICAL REVIEW B VOLUME 19, NUMBER 2 15 JANUARY 1979

Scattering matrix method for surface states applied to Al(001)

D. Spanjaard
Laboratoire de Physique des Solides, Université Paris-Sud, Centre d'Orsay, 91405 Orsay, France

D. W. Jepsen and P. M. Marcus
IBM Thomas J. Watson Research Center, P. O. Box 218, Yorktown Heights, New York 10598
(Received 19 July 1978)

An effective high-accuracy method for finding surface states or surface resonances of a given crystal potential, based on locating singularities of the scattering matrix of the semi-infinite crystal, is described and illustrated by detailed calculations. The method is applied to Al(001) using a potential that is known to give reasonable results for bulk and surface properties; the effects of various transitional potentials between bulk and vacuum are also studied. A large number and a great variety of surface states are found, which can be classified by the types and numbers of overlapping energy gaps of the bulk band structure in which they occur. Seven types are found between the muffin-tin zero and the vacuum level, and surface states are present in almost all the energy gaps in that energy range. For the most widely distributed types in the two-dimensional Brillouin zone, densities of surface states in energy are found that include logarithmic singularities. A convenient method is described for calculating such densities of states for states whose energies are given on an arbitrary mesh of points in two dimensions.

I. INTRODUCTION

Surface states on metals have long been studied theoretically, particularly as interest in the electronic structure of surfaces has grown.[1-3] However, only recently has direct experimental observation by field emission and angle-resolved photoemission techniques made the study of surface states an important part of surface physics.[3-6] The calculation of these states is a difficult extension of band theory, requiring both new types of wave function in a periodic potential and the satisfaction of special boundary conditions at an interface and at infinity.

The present work describes and applies an effective method for finding with high accuracy the surface states of the true semi-infinite crystal, and thereby avoids difficulties encountered by methods using eigenvalues of films, such as confusion between surface states and bulk states, and interaction between states on two surfaces. The procedure used here locates surface states as singularities of the scattering matrix, rather than as eigenvalues of a coefficient matrix for stationary-state equations, and is a development of an earlier formulation[7] that found the scattering matrix in the same way as in low-energy electron-diffraction (LEED) theory.

The method is applied to a self-consistent bulk potential for Al, truncated at the (001) surface. This potential is due to Snow,[8] and is known to give reasonable bulk properties and also to give certain surface states in the positions observed by angle-resolved photoemission.[5] A careful search through all the energy gaps between the muffin-tin zero and the vacuum level (12.4 eV higher) reveals the presence of a large number of surface states of a great variety of types. Some seven types are identified by the nature of the gaps in which they occur, notably in gaps at the edge or center of the Brillouin zone (edge gaps) or in gaps between extrema at points inside the zone (inner gaps), or in overlapping gaps of various types up to as many as three—in which case three surface states are present in the overlapping range. A systematic classification is given, including the region of the two-dimensional zone in which each type occurs. For certain surface states, which occur over substantial ranges of the Brillouin zone, a sufficient number of states is found to permit evaluation of the density of these surface states in energy, including the occurrence of discontinuous jumps and logarithmic singularities in such densities; however, the densities show differences from the densities of functions which exist everywhere in the Brillouin zone.

One interesting part of the analysis, discussed in Sec. IV, concerns the way in which an edge-gap type surface state is continuously transformed into an inner-gap type as a continuous path for k_x and k_y in the surface Brillouin zone is followed. The analysis makes use of the *real line*, a line of solutions of the Schrödinger equation for the given bulk periodic potential with fixed k_x and k_y along which the energy E is real and continuous and traces out all the bands and all the energy gaps as a function of the real and imaginary parts of k_z. As k_x and k_y are varied, the entire real line moves in this space with coordinates E and complex k_z. When an edge gap turns into an inner gap, two real lines first

intersect and then pull apart with a different interconnection of the four segments; the surface state is carried with the gap. A sharp criterion is shown to exist for the transformation from an edge-gap-type to an inner-gap-type surface state, when the k_z values of the Bloch waves making up the surface state abruptly change character.

In Sec. II the scattering matrix method for location of surface states is formulated, and in Sec. III the computational procedures are discussed, including a particularly useful form of the singularity condition which avoids certain numerical complications. It is shown that the method can locate resonant states almost as easily as true surface states, and a numerical example is given. Detailed results for Al are given in Sec. IV, including the ranges in k space for each type of surface state and the location in the band structure for the most prevalent types. Some states that penetrate very deeply into the lattice are found, which would be difficult to locate by methods based on films. Some comparisons of these results with the work of Caruthers, Kleinman, and Alldredge[9] on Al(001) by a different method (based on films) and a different potential (a surface-modified pseudopotential) are made; the two sets of results show a satisfactory general agreement, but a few differences that could permit discrimination between potentials.

Section V obtains and discusses the density of surface states in energy calculated by a special triangular-cell modification of the Gilat-Raubenheimer method, which is convenient for carrying out integrations of a function defined at an arbitrary set of points in two dimensions (hence can be efficiently improved to a desired accuracy by adding points in the appropriate regions). The theory of this method, as well as a simple discussion of the Van Hove singularities for two-dimensional distributions are given in Appendices I and II. The effects of various transition potentials between bulk and vacuum, including a simple smooth transition based on jellium work are studied in Sec. VI. It is concluded that shifts in the energy scale of the surface states can be produced, but not significant shifts in number and distribution of surface states. This conclusion is in agreement with Forstmann,[2] and indicates that the self-consistent potential for the Al surface, when found, would probably show similar small differences from the present calculation.

II. FORMULATION OF THE SURFACE-STATE CONDITION

The method used to calculate surface states makes use of the procedures developed for the LEED problem.[7,10] Consider a set of incident plane waves of given energy E and reduced component of wave number $\vec{k}_\rho$ parallel to the surface of the semi-infinite crystal, whose amplitudes form the components of a vector α^+ (Fig. 1). Let the amplitudes of the reflected waves, all of which have the same E and $\vec{k}_\rho$, form a vector α^-, which is linearly related to α^+ by the reflection matrix R

$$\alpha^- = R\alpha^+. \tag{1}$$

For a surface state to exist, the amplitudes α^- must be finite even when α^+ vanishes, hence the determinant of R must be singular, i.e., we seek a solution of the homogeneous equation $R\alpha^+ = 0$.

The matrix R is in fact found in the solution of the LEED problem, since the vector α^- gives the amplitudes of the diffracted beams from the crystal surface. The layer Korringa-Kohn-Rostoker (layer KKR) method applies multiple-scattering theory in the KKR form to a single atomic layer, assumed periodic in the $\vec{\rho}$ or x-y plane, to give the scattering from a semi-infinite crystal. We give a brief summary of the method in order to point out special features relevant to the surface state problem.

Consider the crystal to be dissected into a succession of elementary layers, each of which is periodic in the plane of the layer, and, for convenience, imagine these layers separated by infinitesimal vacuum spaces. Then the wave function may be expanded in plane waves in the $\vec{\rho}$ plane in the form

$$\psi(\vec{r}) = \sum_K \psi_K(z) e^{i(\vec{k}_\rho + \vec{K}_\rho)\cdot\vec{\rho}}, \tag{2}$$

where $\vec{k}_\rho$ is the component of the wave vector $\vec{k}$ in the $\vec{\rho}$ plane, the $\vec{K}_\rho$ are the reciprocal-lattice vectors of the two-dimensional lattice at z, and the summation is over all the $\vec{K}_\rho$. In the vacuum space between layers (at z), $\psi_K(z)$ may be regarded as the sum of two running waves in the $+z$ and $-z$ di-

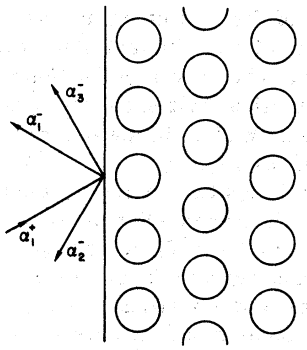

FIG. 1. Incident and reflected beams from a semi-infinite crystal.

rections with amplitudes α_K^+ and α_K^-

$$\psi_K(z) = \alpha_K^+(z)e^{ik_z(K)z} + \alpha_K^-(z)e^{-ik_z(K)z}, \tag{3}$$

where $k_z(K) = (E - |\vec{k}_\rho + \vec{K}_\rho|^2)^{1/2}$.

Substitution of (2) into the Schrödinger equation leads to coupled differential equations for the amplitudes $\psi_K(z)$

$$\frac{d^2\psi_K(z)}{dz^2} = -k_z^2\psi_K(z) + \sum_{K'} V_{(K-K')}(z)\psi_{K'}(z), \tag{4}$$

where

$$V_K(z) = \frac{1}{A_\rho}\int\int_{A_\rho} V(\vec{\rho}, z)e^{-i\vec{K}\cdot\vec{\rho}}\, d^2\rho \tag{5}$$

and A_ρ is the area of the unit cell in the $\vec{\rho}$ plane.

Equation (4) can be compactly written in matrix form

$$d\Phi(z)/dz = A\Phi(z). \tag{6}$$

When (2) contains n plane waves (n-beam representation), Φ has the $2n$ components ψ_{K_1}, $\psi_{K_2}, \ldots, \psi_{K_N}$, $\partial\psi_{K_1}/\partial z$, $\partial\psi_{K_2}/\partial z, \ldots, \partial\psi_{K_N}/\partial z$ and A is a $2n\times 2n$ matrix depending on V_K and k_z. The formal solution of (6) can be written

$$\Phi(z) = P(z, z_0)\Phi(z_0), \tag{7}$$

where P is the matricant of the system,[11] which has been called the propagation matrix since P propagates the wave function from z_0 to z. The particular case in which P propagates the wave function from one side of a layer to the other side is of interest here. The single-layer P matrix is simply related to the usual scattering matrix of a layer (the matrix relating outgoing plane waves to incoming plane waves), which may be found by the layer-KKR method.[10] We assume here that P has been found as in the LEED calculations and refer to that work for details of the layer-KKR method.

The eigenvectors of the single-layer P matrix give the "generalized" Bloch waves of the crystal made up by repetition of that layer, i.e., generalized to include attenuating waves. If ψ^B is a Bloch wave (of $2n$ components) then

$$P(z_0 + L_z, z_0)\psi^B(z_0) = e^{ik_zL_z}\psi^B(z_0), \tag{8}$$

where L_z is the thickness of the layer and k_z may be complex. Let B denote the matrix that diagonalizes P, so that a matrix relation holds of the form

$$B^{-1}PB = \Lambda, \tag{9}$$

where Λ is diagonal. Then any $\Phi(z)$ can be resolved into Bloch waves by multiplying by B^{-1} on the left. The rows of B^{-1} are made up of the left eigenvectors of P and it is convenient to order them so that those corresponding to waves carrying flux into the solid (toward $+z$) or attenuating toward $+z$ lie in the upper half of the B^{-1} matrix while the others lie in the lower half. As there is no wave carrying flux from inside the solid, we must have

$$B^{-1}\Phi = \gamma = \begin{pmatrix} X \\ 0 \end{pmatrix}, \tag{10}$$

where the lower half of the Bloch wave amplitude vector γ vanishes. The wave function may similarly be expanded in vacuum in plane waves (the Bloch waves of the vacuum) in the form

$$\Phi = F\alpha = F\begin{pmatrix} \alpha^+ \\ \alpha^- \end{pmatrix}, \tag{11}$$

where F is readily found from (3).

If we now introduce a matrix P_{surf} that propagates the wave function from vacuum through the transition region between vacuum and bulk, the matching equations expressing continuity of Φ can be written, using (10) and (11),

$$\begin{pmatrix} X \\ 0 \end{pmatrix} = B^{-1}P_{\text{surf}}F\begin{pmatrix} \alpha^+ \\ \alpha^- \end{pmatrix} = \begin{pmatrix} G & H \\ M & L \end{pmatrix}\begin{pmatrix} \alpha^+ \\ \alpha^- \end{pmatrix}. \tag{12}$$

Thus $\alpha^- = L^{-1}M\alpha^+$ and R in (1) is the known matrix $L^{-1}M$, thus the surface-state condition is

$$\det(L^{-1}M) = \infty. \tag{13}$$

In fact, the condition $\det(L) = 0$ is sufficient to find the surface state, but for practical reasons it is better to calculate $L^{-1}M$, which has a simple physical interpretation as a reflection matrix. The determinant of $L^{-1}M$ is a well-behaved function of energy, independent of the ordering and normalization of the eigenvectors used to form it; and hence easier to handle than $\det(L)$.

This formulation, yielding the condition (13), has been systematically applied to the (001) face of aluminum.

III. COMPUTATIONAL DETAILS

In the calculation made here for Al(001) using a standard muffin-tin potential for aluminum[8] and studying energies between the muffin-tin zero and the vacuum level, 12.4 eV higher, accurate band structures can be found with 13 beams, i.e., $n = 13$. At given k_x, k_y values, a systematic search procedure for surface states calculates $\det(L^{-1}M)$ at a mesh of E values from 0 to 12.4 eV with a typical spacing $\Delta E = 0.02$ eV and tests for the change of sign in the real and imaginary parts that must occur at a singularity. When a change in sign occurs, the ΔE is divided by a factor, typically 10, the sign of ΔE is reversed, and a new series of steps is made in order to locate the change of sign again on the smaller mesh, continuing the process until the position of the sign change is located to a desired precision, say $\Delta E/10^6$. If a plot of $S/$

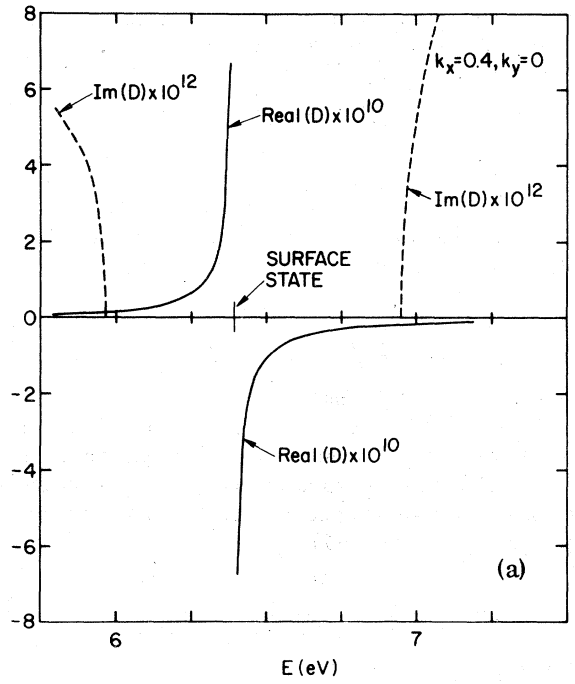

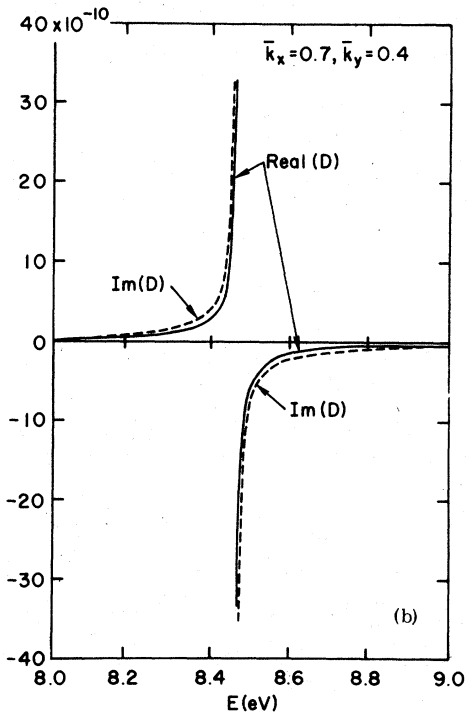

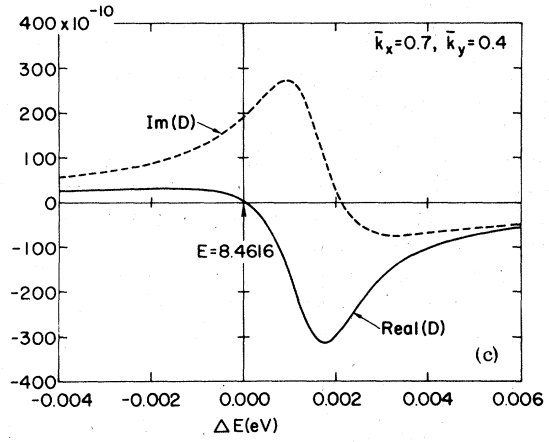

FIG. 2. (a) Real and imaginary parts of $\det(L^{-1}M)$ vs E in the neighborhood of a surface state existing in a true gap. (b) Real and imaginary parts of $\det(L^{-1}M)$ vs E in the neighborhood of a resonance. (c) Same as (b) on an expanded energy scale. [$D \equiv \det(L^{-1}M)$.]

$|\det(L^{-1}M)|$ vs E, where S is the sign of the real part of $\det(L^{-1}M)$, gives a smooth curve through zero, then a pole of $\det(L^{-1}M)$ has been found and a surface state located.

In general, the surface state lies in an absolute gap, i.e., at an energy at which no propagating Bloch function exists for the given k_x and k_y, although two exceptions are noted later. If the transition region is simply an abrupt step between the bulk potential and the vacuum level, then $\det(L^{-1}M)$ is real and the above procedure is simplified. The typical behavior of $\det(L^{-1}M)$ is shown in Fig. 2(a) for $\bar{k}_x = 0.4, \bar{k}_y = 0$. Note that the surface state is in the center of the gap but its occurrence is already indicated by the behavior of $\mathrm{Re}[\det(L^{-1}M)]$ near the edges of the gap. When $\det(L^{-1}M)$ does not have a true pole on the real E axis, but has one at a nearby complex E value, we have a "leaky" surface state or a resonance.[1,12] Such a state has no singularity for real E values, but shows the typical resonance curves illustrated in Fig. 2(b) around $E = 8.5$ eV at $\bar{k}_x = 0.2, \bar{k}_y = 0.4$. This state in fact exists in a gap, but propagating Bloch states exist at that same energy and k_x and k_y values.

A difficulty in locating the surface state develops if the singularity of $\det(L^{-1}M)$ is very near a zero of $\det(L^{-1}M)$, so that a coarse mesh in E misses the change of sign due to the singularity because of

the double change of sign. To avoid these oversights, it is necessary to keep track of the zeros of $\det(L^{-1}M)$ as $\vec{k}$ moves in the Brillouin zone, starting from regions in which the singularity and the zero are well-separated.

IV. DETAILED RESULTS FOR Al

The self-consistent muffin-tin potential for Al found by Snow[8] and used here has been shown to give reasonable Fermi-surface results[13] and LEED spectra.[10,14] In addition, recent work by Gartland and Slagsvold[5] using angle-resolved photoemission has found the surface state along $\Gamma\bar{X}$ classified as A type later in this section to be within 0.3 eV of the position calculated here from the Snow potential. However, unlike the LEED calculations, which add an imaginary part to the potential, no absorption to represent inelastic scattering of electrons need be introduced here. The electronic states should in any case be quite sharp because they are within a few volts of the Fermi level. The initial calculations assumed an abrupt transition region between bulk crystal and vacuum, i.e., a jump in the potential of 12.4 eV at a plane midway between atomic planes, the sum of the Fermi energy (8.2 eV) and the work function of the (001) face (4.24 ± 0.3 eV); in agreement with Snow, the lattice parameter (side of the cubic cell) was taken as $a = 7.6524$ a.u.

The square two-dimensional Brillouin zone for the (001) surface of the face-centered cubic lattice

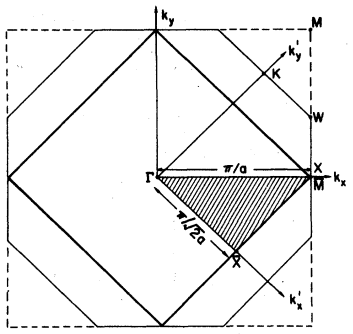

FIG. 3. Two-dimensional Brillouin zone for the (001) face of a fcc lattice embedded in the corresponding three-dimensional Brillouin zone.

is shown in Fig. 3 (heavy lines) embedded in the xy projection of the three-dimensional zone. Note that the k_x', k_y' axes used for the two-dimensional zone are at 45° to the cubic k_x, k_y axes. Symmetry allows us to restrict attention to one-eighth of the square, namely to the irreducible shaded triangle $\Gamma\bar{X}\bar{M}$.

In Figs. 4(a)–4(c) are shown three sets of plots of the three-dimensional band structures $E(k_z)$ at k_x, k_y values along the edges of the irreducible triangle covering the relevant range of energies. These band plots provide a valuable guide to locating and classifying the surface states, which are marked in the energy gaps in the figures, and, in fact, for this study 66 such plots were made on a

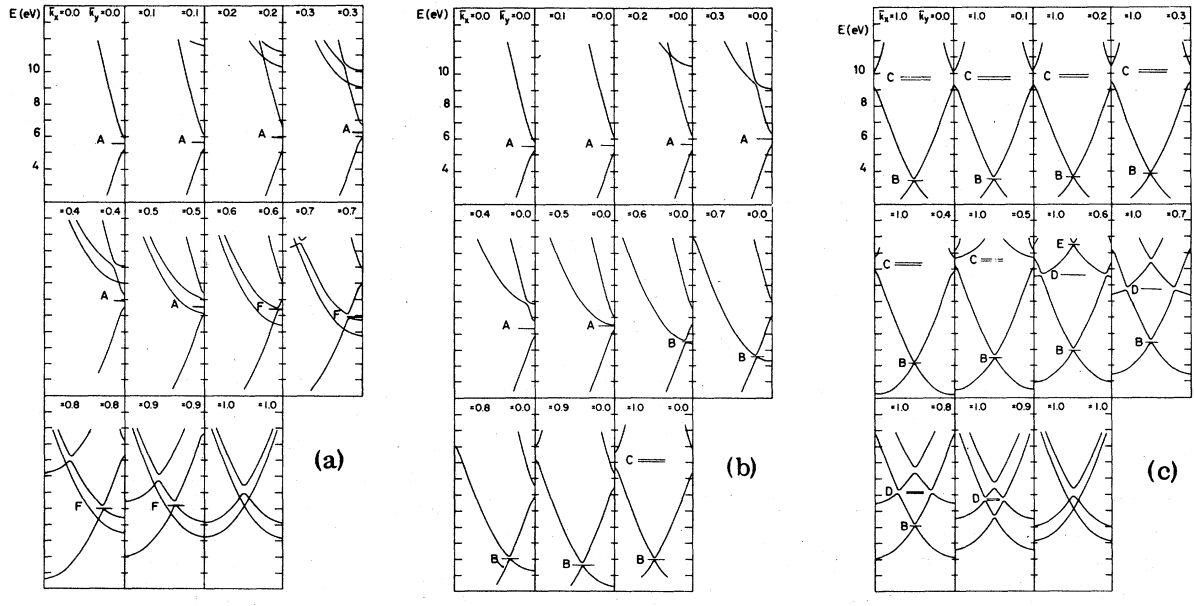

FIG. 4. (a) Plots of the three-dimensional band structures $E(k_z)$ at $\bar{k}_x$, $\bar{k}_y$ values along the $\Gamma\bar{M}$ direction. (b) Plots of the three-dimensional band structures $E(k_z)$ at $\bar{k}_x$, $\bar{k}_y$ values along the $\Gamma\bar{X}$ direction. (c) Plots of the three-dimensional band structures $E(k_z)$ at $\bar{k}_x$, $\bar{k}_y$ values along the $\bar{X}\bar{M}$ direction.

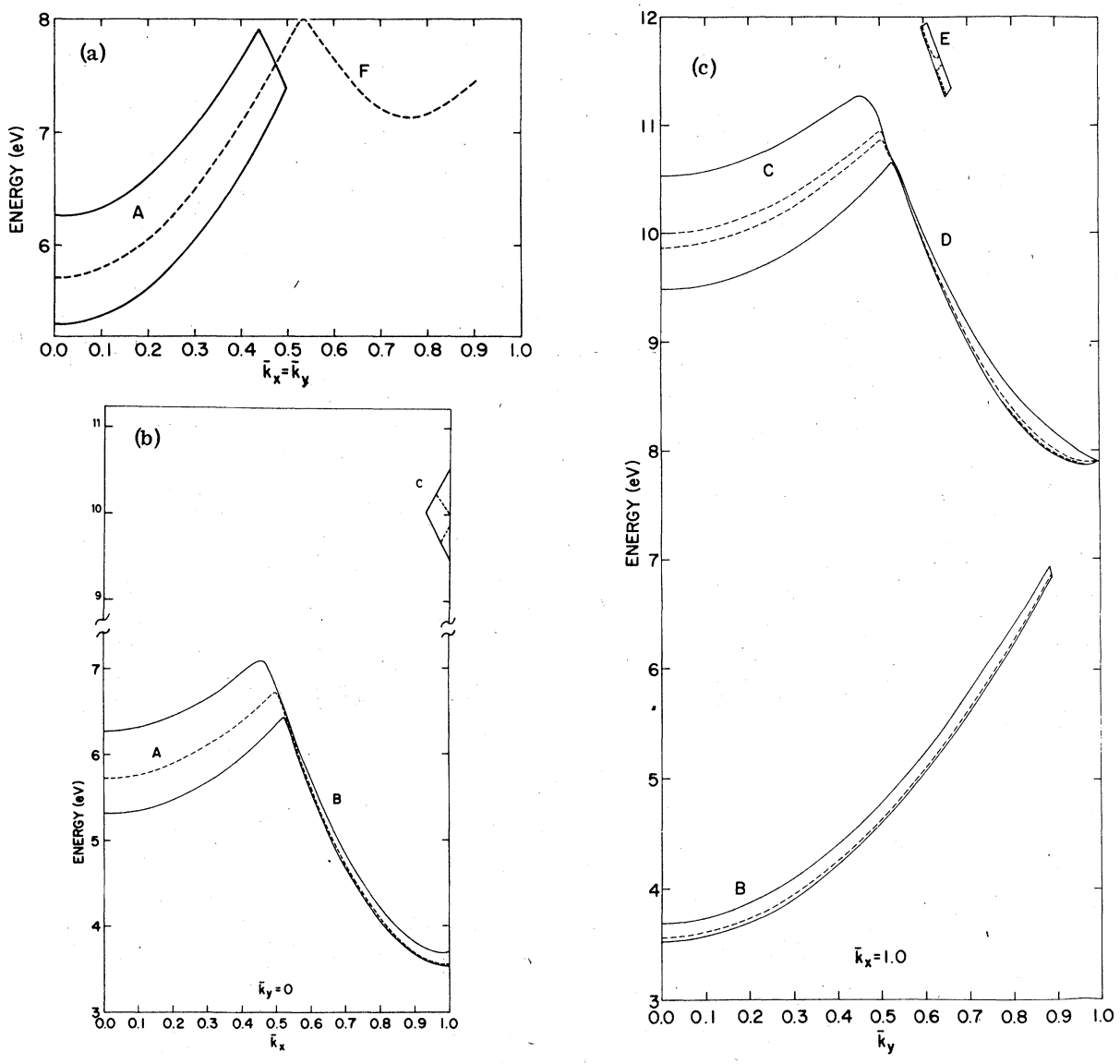

FIG. 5. (a) Variations of the energy of the surface states A and F (and of the corresponding band edges) along the $\Gamma\bar{M}$ direction. (b) Variations of the energy of the surface states A, B, and C (and of the corresponding band edges) along the $\Gamma\bar{X}$ direction. (c) Variations of the energy of the surface states B, C, D, E (and of the corresponding band edges) along the $\bar{X}\bar{M}$ direction.

uniform mesh over the Brillouin zone with a spacing of $\Delta\bar{k}_x, \Delta\bar{k}_y = 0.1, 0.1$, in terms of the reduced coordinates

$$\bar{k}_x \equiv k_x' a\sqrt{2}/\pi\,, \quad \bar{k}_y \equiv k_y' a\sqrt{2}/\pi\,. \tag{14}$$

The continuous variation of the band edges occurring in Fig. 4 and of the corresponding surface states in the gaps belonging to these edges is shown in Figs. 5(a)–5(c). The regions of existence and the characterization of the seven types of surface state (classified according to the number and types of gaps in which they occur) in the energy range studied are indicated on the irreducible triangle in Fig. 6 and listed in Table I. Note that only the A and B states have a sizeable range in $\bar{k}$ space, nearly covering the zone, and each exists in a single absolute energy gap. However, states like C and D require the overlap of (the energy ranges of) two gaps, and have rather limited ranges in $\bar{k}$ space, while the E state requires the overlap of three gaps and has an even more limited range in $\bar{k}$ space. States like F and G exist only along sym-

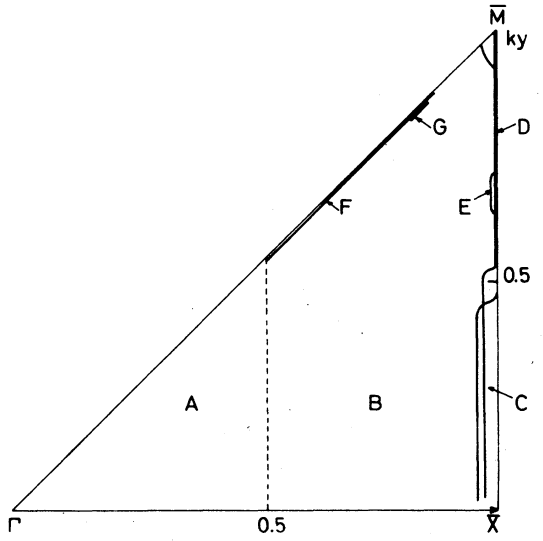

FIG. 6. Regions of existence and labeling of the seven types of surface states in the irreducible two-dimensional Brillouin zone.

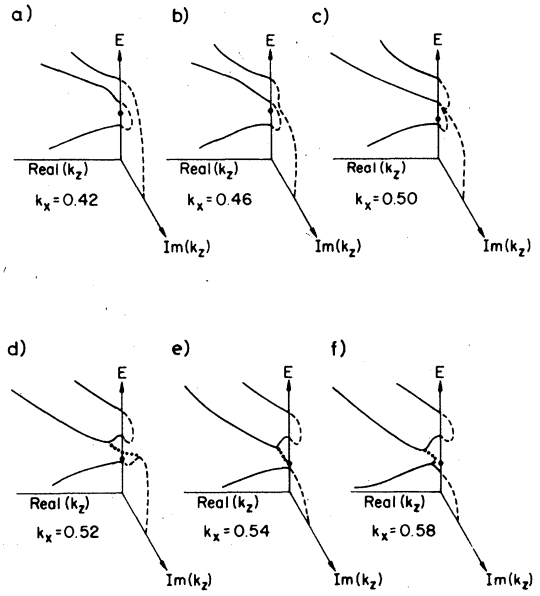

FIG. 7. Perspective plots of the complex band structure at a sequence of points along the $\Gamma\bar{X}$ line going from the region A to the region B.

metry lines, since they achieve stability in spite of the presence of a band of propagating Bloch states at the same energy by the vanishing of the interaction of the surface state with that Bloch state; G has the more limited range in $\bar{k}$ since it requires the overlap of two energy gaps.

It is of interest to note that the A and B states appear to be continuously connected, even though they exist in different types of energy gap (A in edge gaps, B in inner gaps). This continuity can be understood from the band edge plot in Fig. 5(b), which shows that although the gap becomes very narrow, it never closes completely, and the surface state in the gap appears to thread its way continuously between A and B regions without disappearing.[15] At the narrowest part of the gap, the surface state attenuates very slowly, as we shall see in Fig. 8, and is far from localized.

If we move in the Brillouin zone from the A region to the B region, a complicated sequence of

TABLE I. Classification and location of the surface states of Al(001) above the muffin-tin zero.

Label	Nature of energy gap	Symmetry required?	Range in basic triangle of Brillouin zone	Range in energy (in eV above the muffin-tin zero)	Relevant figures and comments
A	Edge	No	$0 \leq \bar{k}_x, \bar{k}_y \leq 0.5$	$5.8 \leq E_A \leq 7.7$	4(a), 4(b), 5(a), 5(b)
B	Inner	No	$0.5 \leq \bar{k}_x, \bar{k}_y \leq 1.0$	$3.6 \leq E_B \leq 7.0$	4(b), 4(c), 5(b), 5(c) continuous with A
C	Two edge	No	$0.97 \leq \bar{k}_x \leq 1.00$, $0 \leq \bar{k}_y < 0.5$	$9.7 \leq E_C \leq 11.0$	4(c), 5(c) long thin area in k near $\bar{k}_x = 1$
D	Two inner	No	$\bar{k}_x \simeq 1.00$, $0.5 \leq k_y \leq 1.00$	$7.9 \leq E_D \leq 10.8$	4(c), 5(b), 5(c) continuous with C, long, very thin area in k near $\bar{k}_x = 1$
E	Two edge and one inner	No	$\bar{k}_x \simeq 1.00$, $0.59 \leq \bar{k}_y \leq 0.66$	$11.3 \leq E_E \leq 11.9$	4(c) (seventh plot), 5(c) small area in k near $\bar{k}_x = 1$
F	One edge then one inner	Yes	$0.47 \leq \bar{k}_x = \bar{k}_y \leq 0.92$	$7.1 \leq E_F \leq 8.0$	4(a), 5(a) only along a symmetry line in k
G	One edge and one inner	Yes	$0.76 \leq \bar{k}_x = \bar{k}_y < 0.78$	$10.8 \leq E_G < 11.0$	4(a) (between plots 8 and 9) symmetry line, small range

transformations of the bands takes place as the band gap at the zone boundary containing the A state is narrowed by the movement of another band across it and converted into a band gap inside the zone. These transformations are made easier to follow by studying the behavior of the entire real lines, of which the bands are segments, in the space where coordinates are E and the real and imaginary parts of k_z. In Fig. 7 we give a sequence of perspective plots of two real lines, i.e., of the complex band structure at a sequence of points on the $\Gamma\bar{X}$ line ($\bar{k}_y = 0$), which cross from the A region to the B region. The real lines, which run continuously from $E = -\infty$ to $E = +\infty$, are made up of segments in the E-Re(k_z) plane which form the usual energy bands, and connecting segments in the E-Im(k_z) plane, as well as space curves [shown dotted in Figs. 7(d)–7(f)]; this curve finally became a real line connecting band edges inside the zone in Fig. 7(e). This sequence exhibits the way in which an edge gap is transformed into an inner gap in a prototype situation in which a band moves across the edge gap formed by two other bands, while continuity of real lines is preserved throughout. The behavior in Figs. 7 and 5(b) is in contrast to the behavior shown in Fig. 5(a), where the moving band does not interact with the bands forming the edge gap, hence cuts off the gap sharply and completely as A states turn into F states. However, later, the nonabsolute gap in which the F state exists is crossed by another, interacting, band and the gap is pulled away from the zone edge as in the A to B transformation.

Further insight into the behavior of a surface state as it transforms from type A to type B is provided by examining the decay factor of the surface state, which we define as the relative decrease in intensity of the most slowly attenuating Bloch wave component of the surface state after one lattice spacing (distance $\frac{1}{2}a$). These decay factors are plotted in Fig. 8 along the $\Gamma\bar{X}$ symmetry line. The plot shows that at the edge of the A states ($\bar{k}_x \cong 0.5$) the attenuation rate becomes very small (decay factor very near unity). A second important slowly decaying component is added to the first in this region and the two components merge with a value of about 0.8 near the point at which the lower band edge pulls away from the zone edge.

Although the A states appear to go continuously into the B states, they can be distinguished in general by the type of gap in which each exists—edge or inner—as in done above. However, this distinction does not provide a sharp line of separation on the $\bar{k}$ plane, since the separation takes place over a range in $\bar{k}$ as first one band edge and then, at a different $\bar{k}$, the other band edge pulls away from the edge of the zone. The transformation

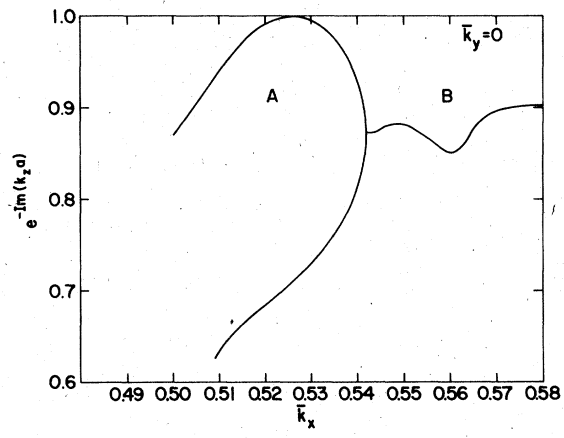

FIG. 8. Decay factor of the surface state A and B along the $\Gamma\bar{X}$ line.

from type A state to type B can be arbitrarily chosen as the point where one or the other band edge pulls away into the interior, or where the energy gap is narrowest, but the sharpest criterion appears to be the point of merger of two attenuating waves to a single (degenerate) attenuating wave. This merger occurs when the surface state is at an energy at which the real line starts into the E-Re(k_z) plane, i.e., when the relevant part of the gap, the part containing the surface state, is an inner type gap. This point is shown in Fig. 8 at $\bar{k}_x = 0.54$.

These results constitute an exhaustive survey of the entire Brillouin zone for surface states, a survey made possible by the construction of the band structures at a dense mesh of points in the zone. All absolute gaps can then be located in the energy range surveyed, including cases in which such gaps open and close between mesh points (e.g., the G states), since the mesh points are closely spaced enough to follow the changes by continuity. Surface states have been found in all absolute gaps both edge and inner type, and in all nonabsolute gaps, both edge and inner type, which are cut off by a band which is noninteracting with the gap bands due to symmetry—with one exception: at $\bar{k}_x, \bar{k}_y = 1.0, 1.0$, no surface state was found in an inner gap cut off by a noninteracting band, although allowed. Thus the results are consistent with Shockley's work,[16] which predicts the existence of a surface state inside an edge gap, provided that the matrix element responsible for the gap has the right sign, and also with Forstmann's work,[17] which predicts the existence of a surface state in inner gaps provided that the gap is due to an interaction not present in the surface barrier, and that the transition region of the potential is an abrupt step at one of the mirror planes of the crystal.

It is useful to compare our results on Al(001) to

those obtained by Caruthers, Kleinman, and Aldredge[9] (CKA) with a different method (one which finds thin-film eigenvalues), and a different potential (one derived from a bulk pseudopotential modified by a transition potential to vacuum based on the jellium work). They found the gaps along the symmetry lines and list a few surface states at Γ, $\bar{X}$, and $\bar{M}$. The positions of the gaps along the $\Gamma\bar{M}$, $\bar{M}\bar{X}$, and $\bar{X}\Gamma$ lines of the two-dimensional zones are very similar in the two calculations. However, on $\bar{M}\bar{X}$, the gap E is missing in CKA. The surface states found at Γ and $\bar{X}$ are in agreement, but a surface state found by CKA at $\bar{M}$ does not exist in our calculation. As shown in Fig. 4(a), the surface states B and D have vanished at $\bar{M}$ as a result of the closing of their respective gaps. However, there is still the possibility of a surface state about 8 eV above the muffin-tin zero in a nonabsolute gap (the gap is closed by two Bloch waves which do not mix with the bands forming the gap). It is possible that a change in the surface potential would produce a surface state in this gap, which would become a surface resonance around the $\bar{M}$ point (outside the $\Gamma\bar{M}$ line).

V. DISTRIBUTION OF SURFACE STATES

In Sec. IV, we have been concerned with surveying, classifying and discussing the relations among the surface states on Al(001). Now we put together all the individual results to give a quantitative description of the distribution of these surface states. The most numerous states are the A and B states, which together almost cover the Brillouin zone, hence we focus attention on them, but also give some results on the C states. A comprehensive view of the distribution of A and B states in $\bar{k}$ space is provided by the contour lines of constant surface-state energy in the irreducible triangle in Fig. 9. Note the following features of these contour lines, which correspond to features of the density of states in energy to be given later:

(i) the minimum at $(\bar{k}_x, \bar{k}_y) = (1, 0)$, $E_s = 3.564$ eV;

(ii) the (local) minimum at $(\bar{k}_x, \bar{k}_y) = (0, 0)$, $E_s = 5.718$ eV;

(iii) the saddle point at $(\bar{k}_x, \bar{k}_y) = (0.496, 0)$, $E_s = 6.715$ eV;

(iv) the maximum near $(\bar{k}_x, \bar{k}_y) = (0.5, 0.5)$, $E_s = 7.6$ eV;

(v) the cutting off of the states in the vicinity of $(\bar{k}_x, \bar{k}_y) = (1, 1)$ produced by the closing of the B-state energy gap, so that the maximum point is not attained.

A more compact view of the distribution of surface states than the contour line plots is provided by the density of states in energy as a function of energy. We calculate this function using a modification of the Gilat-Raubenheimer method[18] based on triangular cells, in each of which the linearity of $E_s(k_x, k_y)$ is assumed. The method is simple and flexible, since additional triangles are readily introduced in regions where E_s varies more rapidly. The procedure used by Hoffstein[19] appears to be very similar, but he does not give any details or specific formulas, so that we have put these formulas into Appendix A for reference.

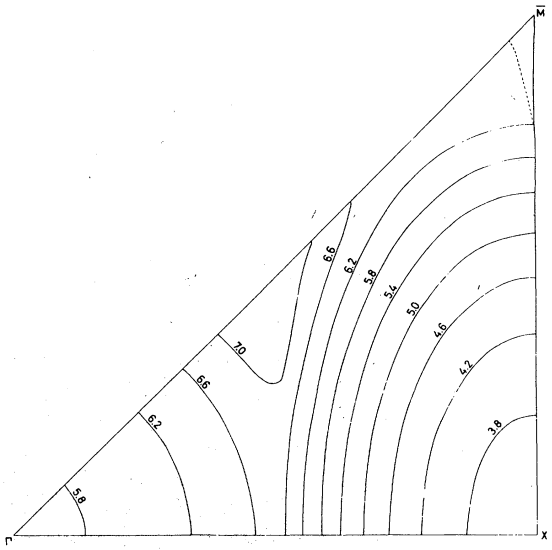

FIG. 9. Contour lines of constant surface-state energy in the irreducible two-dimensional Brillouin zone.

The results obtained for the density of A states ρ_A, the density of B states ρ_B, and for their combined contributions by means of the triangular Gilat-Raubenheimer method using about 150 triangles in each region, are shown in Fig. 10. For

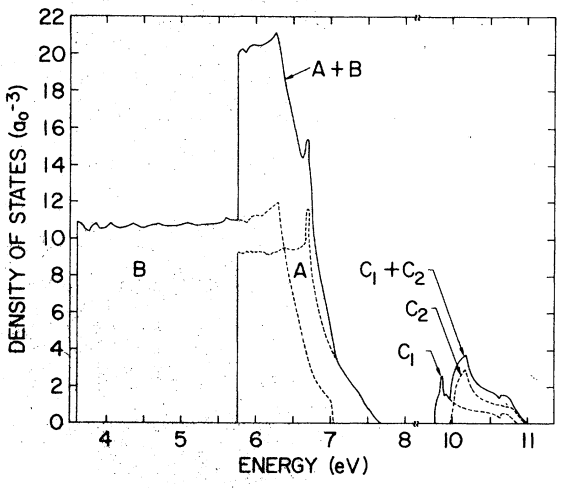

FIG. 10. Density of surface states.

convenience in relating the contour lines to the density of states, we give in Appendix B a summary of the general relationships between level lines of a function of two coordinates and the density of the area in that function (i.e., area per unit change in the function value). Note first the overall flatness of both the A and B state densities, which is related to the nearly parabolic dispersion curves of E_s against $\vec{k}$ that we see along symmetry lines in Figs. 5(a) and 5(b). Thus when E is a quadratic function of k_x and k_y in the vicinity of a maximum or minimum point, the general formulas (B4) and (B5) show that $\rho(E)$ is linear in E, starting from a finite jump at the maximum or minimum point. The discontinuities in ρ_A at $E=3.56$ and ρ_B at $E=5.72$ eV correspond to the minima noted in features (i) and (ii) above. The logarithmic singularity in ρ_A at $E=6.715$ corresponds to the saddle point noted in feature (iii), in accordance with (B6). Finally, the gradual falloff of ρ_B on the high-energy side corresponds to the cutoff of the maximum point noted in feature (v), but the gradual falloff of ρ_A, even though the maximum of feature (iv) is attained, arises from the special shape of the contour lines as they approach the minimum. Essentially the contour lines each have a cusp and the maximum lies on the line of cusps (i.e., is the top of a sharp ridge rather than a rounded hill). It is easy to see from (B1) and (B2) that if E is linear in k_x and k_y as the maximum E_m is approached, then $\rho_A(E)$ is linear in $E-E_m$. Finally, we note that our results are analogous to the results of Hoffstein,[19] who uses a very simple pseudopotential. However, Hoffstein does not obtain a singularity, which could be explained by a small difference in the states given by his potential.

VI. VARIATION OF SURFACE STATES WITH THE SURFACE POTENTIAL

Calculations of the variation in energy of the surface states with the height and position of the step barrier have been performed for some points of the Brillouin zone.

In Fig. 11, we show results for the surface state energy at the Γ point. When the step barrier moves away from the last layer of atoms, the energy of the surface state decreases and vice versa. This effect has a simple physical interpretation, i.e., when the barrier moves away from the last layer of atoms, the wave function needs to vary less rapidly in order to match the decaying wave in vacuum and therefore the energy of the surface state is lowered. Similarly, if we increase the height of the barrier the energy of the surface state increases.

In Fig. 11, we also compare our results to the

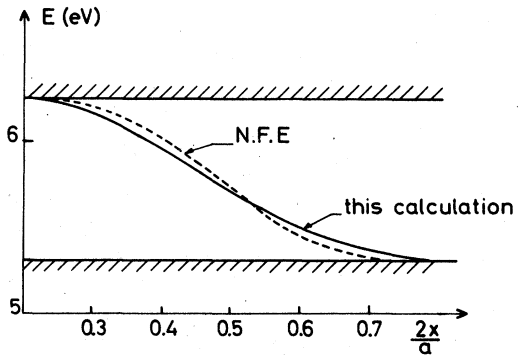

FIG. 11. Energy of the surface state A at the Γ point as a function of the step barrier position relative to the last layer of nuclei. The dotted line corresponds to results using a nearly-free-electron approximation. In $2x/a$, x is the position of the sharp step with respect to the position of the last layer of atoms.

nearly-free-electron results of Velicky *et al.*[20]

$$\epsilon_s = |\Delta/\alpha|\cos[gx_0 - 2\cos^{-1}(\tfrac{1}{2}gV_0^{-1/2})]\,,$$

provided

$$0 \leq gx_0 - 2\cos^{-1}(\tfrac{1}{2}gV_0^{-1/2}) \leq \pi\,,$$

where ϵ_s measures the surface state energy from the middle of the gap, Δ is the width of the gap (0.96 eV at the Γ point), x_0 is the position of the barrier with respect to the position of the last layer of atoms, V_0 is the distance in energy from the bottom of the lower nearly-free-electron band to the top of the potential barrier (approximated here as 15.18 eV), and g is equal to $2\pi/a$. It is clear that this formula gives a fair approximation of our results.

In addition, calculations have been made using a smooth potential barrier of the form $V=\frac{1}{2}V_1[\tanh(x/2t)+1]$. The exact solution of the Schrödinger equation for such a potential has been given by Eckart.[21] In order to solve our matching problem we fit the Eckart wave function and its derivative to the bulk wave function in the plane wave representation at the sites of last layer of atoms. The results for the Γ point are shown in Fig. 12, where the energy of the surface states is plotted against t for several values of the distance between the inflexion point of the surface potential and the sites of the last layer of atoms. Calculations made for some other points inside the Brillouin zone showed very similar behavior.

If we compare the Eckart potential to the Al surface potential as calculated by Lang and Kohn,[22] it is seen that a good fit cannot be obtained because the Lang-Kohn potential is very asymmetric. If the position of the last layer of atoms is taken as half the layer spacing before the end of the continuum

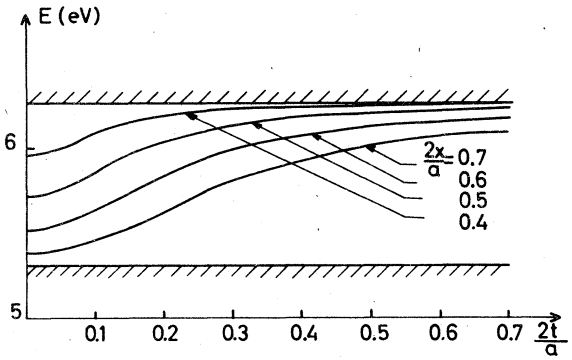

FIG. 12. Energy of the surface state A at the Γ point as function of the width t of the Eckart potential for several positions of the step barrier relative to the last layer of nuclei.

of positive charge, the best fit of the lower part of the two potentials is achieved for $t=0.574$ a.u. (i.e., $t=0.15a/2$) and the position of the inflexion point of the potential is at $x=2.46$ a.u. (i.e., $0.644a/2$) from the last layer sites. An Eckart potential with these parameters would produce a slight shift in energy of the surface states. However, the dispersion relation of the surface states is largely imposed by the gaps (i.e., by the bulk potential) and therefore the effect produced in the density of states would be a shift of the energy scale rather than a change of shape.

APPENDIX A: CALCULATION OF THE DENSITY OF STATES

A simplified version of the Gilat-Raubenheimer method based on triangles was used to calculate the density of states. Our procedure is the two-dimentional analog of the method of Lehmann and Taut.[23] A similar procedure was used by Hoffstein.[19] The surface Brillouin zone was divided into a mesh of small triangles of arbitrary shape and a contribution to the density of states as a function of energy was calculated from each triangle. A linear fit to the dispersion of surface state energy with k was used within each triangle. The results obtained from all the triangles were summed to get a result for the complete density of states. Those triangles in which the linear fit proved to be inaccurate were divided into smaller triangles and the result resummed until a reasonable approximation to the density of states was obtained.

If the surface state energy varies linearly across a triangle it can be represented by

$$E(k)=\lambda_1 E_1+\lambda_2 E_2+\lambda_3 E_3\,, \tag{A1}$$

where E_1, E_2, and E_3 are the energies at the vertices of the triangle and λ_1, λ_2, and λ_3 are baricentric coordinates for points of the triangle so that

$$\vec{k}=\lambda_1\vec{k}_1+\lambda_2\vec{k}_2+\lambda_3\vec{k}_3 \tag{A2}$$

with

$$\sum_i \lambda_1=1\,,\quad \lambda_i>0\,,$$

where $\vec{k}_1$, $\vec{k}_2$, and $\vec{k}_3$ are the k coordinates of the vertices of the triangle. We shall assume for simplicity that the labeling of the vertices of the triangle is chosen so that $E_1<E_2<E_3$. The contribution of this triangle to the density of states is given by

$$\rho(E)=\int\int_{\text{triangle}} \delta(E(k)-E)\,d^2k\,, \tag{A3}$$

which can be easily evaluated by choosing two of the λ's as independent coordinates. One has

$$\rho(E)=2\int_0^1 d\lambda_1\int_0^{1-\lambda_1} d\lambda_2 \times \delta(\lambda_1(E_1-E_3)+\lambda_2(E_2-E_3)+E_3-E)\,, \tag{A4}$$

where Δ is the area of the triangle, which gives

$$\begin{aligned} &E>E_3\,,\quad \rho(E)=0\,,\\ &E_3>E>E_2\,,\quad \rho(E)=\frac{2\Delta}{E_2-E_3}\,\frac{E_3-E}{E_1-E_3}\,,\\ &E_2>E>E_1\,,\quad \rho(E)=\frac{2\Delta}{E_1-E_2}\,\frac{E-E_1}{E_1-E_3}\,,\\ &E_1>E\,,\quad \rho(E)=0\,; \end{aligned} \tag{A5}$$

thus a single triangle gives the contribution to the density of states shown in Fig. 13.

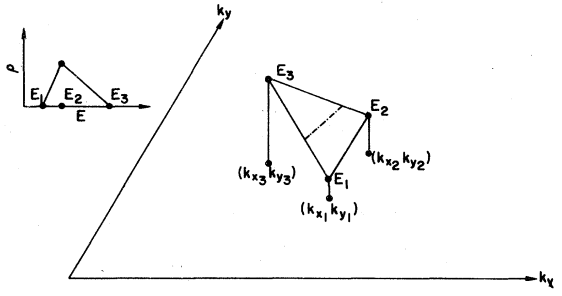

FIG. 13. Elementary triangle in the two-dimensional Brillouin zone and its contribution to the density of surface states as a function of energy.

APPENDIX B: LEVEL LINES OF SURFACE ENERGY AND THE TWO-DIMENSIONAL DENSITY OF STATES

Some convenient relations are obtained below between the level lines along which a function in two dimensions is constant, such as those shown in Fig. 9 for the A- and B-type surface-state energy in the two-dimensional Brillouin zone, and the two-dimensional density of states or density of function values, such as shown for the surface state energy in Fig. 10. These results make apparent the connection between slow function variation (shown by widely separated level lines) at minima, maxima, and to an even greater degree at saddle points and the singularities in the density function given by Van Hove.[24]

Let the equation of a level line of energy E be given with respect to a reference point $\vec{k}_0$, energy E_0, by $\delta E(\delta k, \theta)$ where $\delta E = E - E_0$, $\delta k = |\vec{k} - \vec{k}_0|$, and θ is the polar angle of $\vec{k} - \vec{k}_0$ with respect to the k_x axis. Then the (positive) area of the angular sector around $\vec{k}_0$ from θ_1 to θ_2 and bounded by the level line is

$$A_{12}(E) = \int_{\theta_1}^{\theta_2} \delta k^2(\theta, E)\, \frac{d\theta}{2} \,. \tag{B1}$$

For simplicity consider only sectors in which E is entirely $>E_0$ or entirely $<E_0$. Then the contribution of the level line at E within the sector to the density of states at E is

$$\rho_{12}(E) = \begin{cases} \left(\frac{\partial A_{12}(E)}{\partial E}\right) \Big/ 2\pi^2 \,, & E > E_0 \qquad \text{(B2)} \\ \left(\frac{\partial A_{12}(E)}{\partial E}\right) \Big/ 2\pi^2 \,, & E < E_0 \,, \qquad \text{(B3)} \end{cases}$$

where $2/(2\pi)^2$ is the factor for counting states in $\vec{k}$ space, including a factor of 2 for spin. In addition to the sectoral contribution to the total density of states $\rho(E)$, there will be external contributions from the rest of this contour line or separate contour lines at the same energy, which will be designated $\rho_e(E)$. The results of applying (B2) to (B3) to five cases of interest will now be tabulated.

(i) Minimum point $\vec{k}_m, E_m$, full range sector $\theta_1 = 0$, $\theta_2 = 2\pi$:

$$\delta E = \delta k^2(a^2 \cos^2\theta + b^2 \sin^2\theta) + \delta k^3 f(\theta) + O(\delta k^4) \,, \quad E \geq E_m \,,$$

$$A_{12}(E) = \frac{\delta E}{2} \int_0^{2\pi} \frac{d\theta}{a^2 \cos^2\theta + b^2 \sin^2\theta} + O(\delta E^2) = \pi \delta E/ab + O(\delta E^2) \,,$$

$$\rho(E) = \begin{cases} \rho_e(E) \,, & E < E_m \\ \rho_e(E) + \frac{1}{2}\pi ab + O(\delta E) \,, & E > E_m \,. \end{cases} \tag{B4}$$

At E_m, $\rho_e(E)$ will not in general show sharp behavior, so that a discontinuous upward jump in $\rho(E)$ takes place at E_m, followed by a rise (or fall) linear in δE. The term $\delta k^3 f(\theta)$ in the relation between δE and δk, where $f(\theta)$ is made up of terms like $\cos^3\theta$, $\cos^2\theta \sin\theta$, etc...., if E is analytic at $\vec{k}_0$, cancel out in the integration over θ from 0 to 2π, and the term in δk^4 provides the term of order δE^2 in $A_M(E)$.

(ii) Maximum point, $\vec{k}_M$, E_M, full-range sector $\theta_1 = 0$, $\theta_2 = 2\pi$:

$$\delta E = -(\delta k)^2(a^2 \cos^2\theta + b^2 \sin^2\theta) + \delta k^3 f(\theta) + O(\delta k^4) \,, \quad E < E_M \,,$$

$$A_{12}(E) = -\frac{\delta E}{2} \int_0^{2\pi} \frac{d\theta}{a^2 \cos^2\theta + b^2 \sin^2\theta} + O(\delta E^2) = -\pi \delta E/ab + O(\delta E^2) \,,$$

hence, using (B3),

$$\rho(E) = \begin{cases} \rho_e(E) + \frac{1}{2}\pi ab + O(\delta E) \,, & E < E_M \\ \rho_e(E) \,, & E > E_M \,. \end{cases} \tag{B5}$$

(iii) Saddle point, $\vec{k}_s$, E_s, angular range contains four sectors:

$$\delta E = (\delta k)^2(a^2 \cos^2\theta - b^2 \sin^2\theta) + \delta k^3 f(\theta) + O(\delta k^4) \,.$$

The sectors, in counterclockwise order, are

sector 1: $E < E_s$, $\theta_1 = \theta_{B2}$, $\theta_2 = \theta_{B3}$;

sector 2: $E > E_s$, $\theta_1 = \theta_{B4}$, $\theta_2 = \theta_{B5}$;

sector 3: $E < E_s$, $\theta_1 = \theta_{B6}$, $\theta_2 = \theta_{B7}$;

sector 4: $E > E_s$, $\theta_1 = \theta_{B8}$, $\theta_2 = \theta_{B1}$;

where all the θ_1 and θ_2 values are polar angles of successive intersection points of the level line δE with a cell boundary at radius δk_{Bi},

$$\delta E = (\delta k_{Bi})^2(a^2 \cos^2\theta_{Bi} - b^2 \sin^2\theta_{Bi}) \,, \quad i = 1\text{–}8 \,.$$

Then, to first order in δE,

$$\tan\theta_{Bi} = \begin{cases} a/b - \delta E(a^2 + b^2)/2ab^3 \delta k_{Bi}^2 \,, & i = 1, 2, 5, 6 \\ -a/b + \delta E(a^2 + b^2)/2ab^3 \delta k_{Bi}^2 \,, & i = 3, 4, 7, 8 \,, \end{cases}$$

$$A_1(E) + A_3(E) = \frac{\delta E}{2}\left(\int_{\theta_{B2}}^{\theta_{B3}} + \int_{\theta_{B6}}^{\theta_{B7}}\right) \frac{d\theta}{a^2 \cos^2\theta + b^2 \sin^2\theta} + O(\delta E^2) \,, \quad E < E_s \,,$$

$$A_1(E) + A_3(E) = \left(\frac{\delta E}{4ab}\right) \ln\left|\frac{\tan\theta + a/b}{\tan\theta - a/b}\right|\Bigg|_{\theta_{B2}, \theta_{B6}}^{\theta_{B3}, \theta_{B7}} + O(\delta E^2) \cong \left(\frac{\delta E}{2ab}\right) \ln|\delta E| + C_{13} + O(\delta E^2) \,, \quad E < E_s \,,$$

where C_{13} is a constant depending on a, b and δk_{B1}, δk_{B3}.

Similarly

$$A_2(E)+A_4(E)\cong -(\delta E/2ab)\ln|\delta E|+C_{24}+O(\delta E^2),$$
$$E>E_s,$$
$$\rho(E)=\rho_e(E)-(\ln|\delta E|)/4\pi^2 ab+O(\delta E),$$
$$E<E_s \text{ and } E>E_s. \quad \text{(B6)}$$

(iv) Ordinary point $\vec{k}_0, E_0$, sector $\theta_1-\theta_2$ (on one side of the E_0 level line):

$$\delta E=\delta k(a\cos\theta-b\sin\theta)+O(\delta k^2),$$
$$A(E)=\frac{\delta E^2}{2}\int_{\theta_1}^{\theta_2}\frac{d\theta}{(a\cos\theta-b\sin\theta)^2}+O(\delta E^3),$$

where for definiteness take

$$\theta_2<\theta_0,\quad \theta_1>\theta_0-\pi,$$
$$\theta_0=\begin{cases}\tan^{-1}(a/b), & a/b>0\\ \tan^{-1}(a/b)+\pi, & a/b<0.\end{cases}$$

Using the principal value of $\tan^{-1}$

$$A(E)=\delta[E^2/2(a^2+b^2)][\cot(\theta_1-\theta_0)-\cot(\theta_2-\theta_0)]+O(\delta E^3) \quad \text{(B7)}$$
$$\rho(E)=\rho_e(E)+[\delta E/(a^2+b^2)2\pi^2]\times[\cot(\theta_1-\theta_0)-\cot(\theta_2-\theta_0)]+O(\delta E^2),$$

which agrees with the linear variation of $\rho(E)$ in (A5) and Fig. 13.

(v) Ordinary point $\vec{k}_0, E_0$, full angular range contains two sectors of size π one for $E>E_0$ and one for $E<E_0$:

$$\delta E=\delta k(a\cos\theta-b\sin\theta)$$
$$=\delta k(a^2+b^2)^{1/2}\sin(\theta_0-\theta).$$

Let

$$\theta_2=\theta_0-\epsilon_2,\ \theta_1=\theta_0-\pi+\epsilon_1$$

(then $E>E_0$ for $\epsilon_1, \epsilon_2>0$). Consider the limit of $\rho(E)$ in case (iv) at $\epsilon_1, \epsilon_2\to 0$. Introduce boundary values $\delta k_{B1}, \delta k_{B2}$, where the level line δE crosses the boundary of the cell enclosing $\vec{k}_0$,

$$\delta E=\delta k_{B2}(a^2+b^2)^{1/2}\sin\epsilon_2$$
$$=\delta k_{B1}(a^2+b^2)^{1/2}\sin\epsilon_1.$$

Then, since $\cot\epsilon\to 1/\sin\epsilon$ as $\epsilon\to 0$,

$$\rho(E)=\rho_E(E)+[\delta E/(a^2+b^2)2\pi^2](\cot\epsilon_1+\cot\epsilon_2)$$
$$\cong\rho_E(E)+(\delta k_{B1}+\delta k_{B2})/(a^2+b^2)^{1/2}2\pi^2, \quad \text{(B8)}$$

where $\delta k_{B1}+\delta k_{B2}$ is essentially the diameter of the cell along the level line through $\vec{k}_0$, and $(a^2+b^2)^{1/2}=|\vec{\nabla}_k E|$ at $\vec{k}_0$.

[1]For a recent review, see J. A. Appelbaum and D. R. Hamann, Rev. Mod. Phys. 48, 479 (1976).
[2]F. Forstmann, in *Photoemission from Surfaces*, edited by B. Feuerbacher, B. Fitten, and R. F. Willis (Wiley, New York, 1978), Chap. 8.
[3]P. Soven, E. W. Plummer, and N. Kar, CRC Crit. Rev. Solid State Sci. 6, 111 (1972).
[4]P. O. Gartland and B. J. Slagsvold, Phys. Rev. B 12, 4047 (1975).
[5]P. O. Gartland and B. J. Slagsvold, Solid State Commun. 25, 489 (1978).
[6]C. Noguera, D. Spanjaard, D. W. Jepsen, Y. Ballu, C. Guillot, J. Lecante, J. Paigne, Y. Petroff, R. Pinchaux, P. Thiry, and R. Cinti, Phys. Rev. Lett., 38, 1171 (1977).
[7]P. M. Marcus and D. W. Jepsen, *Computational Methods for Large Molecules and Localized States in Solids*, edited by F. Herman, A. D. McLean, and R. K. Nesbet (Plenum, New York, 1972), p. 235. A similar procedure is formulated by J. B. Pendry and S. J. Gurman, Surf. Sci. 49, 87 (1975).
[8]E. C. Snow, Phys. Rev. 158, 683 (1967).
[9]E. Caruthers, L. Kleinman, and G. P. Alldredge, Phys. Rev. B 8, 4570 (1973).
[10]D. W. Jepsen, P. M. Marcus, and F. Jona, Phys. Rev. B 5, 3933 (1972).
[11]See, e.g., F. R. Gantmacher, *Matrix Theory* (Chelsea, New York, 1960), Vol. II, p. 125.
[12]E. G. McRae, Surf. Sci. 25, 491 (1971).
[13]J. S. Faulkner, Phys. Rev. 178, 914 (1969).
[14]D. W. Jepsen, P. M. Marcus, and F. Jona, Phys. Rev. B 6, 3684 (1972).
[15]The surface state comes extremely close to the band edge and we are unable to exclude the possibility that it disappears completely.
[16]W. Shockley, Phys. Rev. 56, 317 (1939).
[17]F. Forstmann, Z. Phys. 235, 69 (1970).
[18]G. Gilat and L. J. Raubenheimer, Phys. Rev. 144, 390 (1966).
[19]V. Hoffstein, Solid State Commun. 10, 605 (1972).
[20]B. Velicky and J. Bartos, J. Phys. C 4, L104 (1971).
[21]C. Eckart, Phys. Rev. 35, 1303 (1930).
[22]N. D. Lang and W. Kohn, Phys. Rev. B 1, 4555 (1970); 3, 1215 (1971).
[23]G. Lehman and M. Taut, Phys. Status Solidi B 54, 469 (1972).
[24]L. Van Hove, Phys. Rev. 89, 1189 (1953).